

Nature of the magnetic carpet – I. Distribution of magnetic fluxes

C. E. Parnell[★]

School of Mathematics and Statistics, University of St Andrews, North Haugh, St Andrews, Fife KY16 9SS

Accepted 2002 April 26. Received 2002 April 26; in original form 2001 November 26

ABSTRACT

The distribution of magnetic fluxes found in the solar magnetic carpet, the photospheric magnetic field of the quiet-Sun, is investigated. A total of 27 500 concentrations are studied with fluxes ranging between a few times 10^{17} and a few times 10^{20} Mx. A histogram of the fluxes shows that there are more small fluxes and more large fluxes than anticipated by an exponential distribution. However, there are significantly fewer large and small fluxes than a power-law distribution fitted to the middle of the range. Thus, the fluxes are not distributed in the form of either an exponential or a power-law distribution, as previously suggested. Instead, the Weibull distribution, which involves both a power law and an exponential, is found to provide both a statistically good fit to the data and a physically reasonable prediction for the total absolute flux density. The best-fitting Weibull distribution has a Kolmogorov–Smirnov D statistic of approximately 0.07 – well below the 5 per cent significance level and the Weibull distribution predicts the observed total absolute flux densities to within better than 92 per cent.

Physically, the observed distribution of fluxes can be explained as being made up of the following three elements: (i) emergence of new flux over all scales gives rise to an initial exponential distribution (observed); (ii) fragmentation and partial cancellation produce smaller and smaller fluxes thus creating excess small fluxes; (iii) excess large fluxes are created by coalescence and an additional (possibly significant) injection of flux from remnants of active regions. Finally, the equations of ‘magneto-chemistry’ are used to derive suitable forms for the rate of emergence, cancellation, coalescence and fragmentation consistent with a Weibull distribution of fluxes.

Key words: Sun: magnetic fields.

1 INTRODUCTION

Magnetic concentrations of many sizes cover the surface of the Sun from large sunspots with areas of 2×10^9 km² and fluxes of around 10^{21} Mx, down to small-scale network and intranetwork concentrations with areas of just 10^6 km² and fluxes approximately a few times 10^{17} Mx. These concentrations have a dynamic nature, displaying complex behaviour driven by both granular and supergranular motions. Sunspots are thought to originate from the base of the solar convection zone, whilst the ephemeral region and intranetwork fields are believed to be fed from convection or small-scale shear motions just below the surface of the Sun [for a recent discussion on this see Cattaneo (1999)].

The behaviour of small magnetic concentrations on the Sun have been studied since the early 1970s (Harvey & Martin 1973; Harvey, Harvey & Martin 1975; Harvey & Harvey 1976; Harvey 1984; Martin 1984, 1988; Zwaan 1987; Webb et al. 1993; Schrijver & Harvey 1994; Wang 1988; Harvey et al. 2000) using ground-based

data from Kitt Peak Observatory and Big Bear Solar Observatory. Also, more recently data from SOHO/MDI (Scherrer et al. 1995) have been used to probe the nature of the so-called magnetic carpet, the recent name given to the small-scale magnetic field that completely covers the surface of the Sun at solar minimum (Schrijver et al. 1997; Hagenaar et al. 1999; Title 2000; Hagenaar 2001).

There are believed to be three types of small-scale magnetic concentration in the quiet Sun: ephemeral regions, network fields and intranetwork fields. Ephemeral regions were first described by Harvey & Martin (1973) and are clusters of bipolar pairs of magnetic concentrations. Since the initial studies much work has been done to investigate their properties. A recent paper by Hagenaar (2001) describes results from the first automated detection of ephemeral regions where 38 000 events were studied. They range in flux from 2.6×10^{18} to 4.1×10^{20} Mx and the distribution of their fluxes follows an exponential of the form $\exp(-1.6 \times 10^{-19} \text{ Mx}^{-1} \times \phi)$ over the range 10^{19} – 3×10^{19} Mx with an average of 11.3×10^{18} Mx.

Network concentrations are created from the residuals of other flux concentrations (e.g. from individual poles of an ephemeral region) that are swept to the edges of supergranule cells and coalesce to form large concentrations. Therefore, not surprisingly, they are

[★]E-mail: clare@mcs.st-and.ac.uk

typically found at sites of strong down-flow, which are usually at the confluence of two or more supergranule cells. They are found to reach flux strengths of a few times 10^{18} – 10^{19} Mx and have diameters of 10^3 – 10^4 km (Martin 1988).

Intranetwork concentrations, which are also known as inner-network or intracell concentrations, are the smallest of the three types of concentration present in the quiet Sun (Livingston & Harvey 1975; Livi, Martin & Wang 1985; Martin 1984, 1988, 1990; Wang, Zirin & Shi 1985; Wang & Shi 1988; Wang & Zirin 1988; Wang et al. 1995; Zirin 1985, 1987). They have fluxes of between 10^{16} Mx (the detection limit) and 10^{18} Mx and have a mean diameter of about 2×10^3 km, although their size can vary greatly. The flux in these concentrations is fairly weak and cannot be observed well using SOHO/MDI, but several studies using data from the Big Bear Solar Observatory have been carried out.

Schrijver et al. (1997) and Wang et al. (1995) have looked at the distribution of concentration fluxes for network and/or intranetwork concentrations. Schrijver et al. (1997) considered the distribution of fluxes from a very quiet region of the Sun. They found that a single exponential seemed a reasonable fit to the distribution of fluxes over a small range of fluxes. The straight line they fitted to their histogram of fluxes revealed the slope of the exponential distribution to be -10^{-18} Mx $^{-1}$ for concentrations with absolute flux between 1.0×10^{18} and 5.0×10^{18} Mx.

Wang et al. (1995) plotted histograms of distributions of flux concentrations on log–log plots. They calculated the distribution of network and intranetwork fluxes separately and found that these distributions range from 3×10^{15} to 2×10^{18} Mx and from 1×10^{17} to 3×10^{19} Mx, respectively. The distributions showed peaks at about 2×10^{18} and 6×10^{18} Mx. Wang et al. (1995) determined that the fall-offs from the peaks were in the form of power laws with indices of -1.27 and -1.68 , respectively, for the network and intranetwork concentrations, although these fits were not plotted on their graphs. From the histogram of the intranetwork fluxes the drop-off from the peak is not a simple straight line and actually curves, dropping off faster for higher fluxes. This also appears to be the case for the network fluxes, but, since only 500 network fluxes were measured, the histogram has a high degree of scatter.

Since the advent of SOHO/MDI there have been some investigations into ephemeral regions and ephemeral region behaviour, but not many into network concentrations. In this paper, we use

an automated technique to identify concentrations in the quiet Sun, which are tracked for 12 h. The details of the identification algorithm and observations used are given in Section 2, whilst Section 3 investigates the distribution of the magnetic fluxes. In Section 4, a discussion of possible biases in the results is given and a physical interpretation of the distribution is presented. Finally, in Section 5, the results are summarized.

2 OBSERVATIONS AND IDENTIFICATION OF FLUX CONCENTRATIONS

The data set used was taken by SOHO/MDI between 1998 June 13–14 (2 yr after solar minimum) using its high-resolution field of view. The region investigated only covers part of the full (1024×640 pixels) high-resolution field of view and is situated approximately on the disc centre, as shown in Fig. 1. The section chosen has an area of 363×363 arcsec 2 (264×264 Mm 2) and is tracked as it moves across the centre of the Sun for a period of 12.5 h. Level 1.5 data are despiked to remove cosmic ray hits and streaks using the routine ZSPIKE, which is available on SOLARSOFT (SOLARSOFT is a suite of IDL routines including tools to analyse data from both YOHKO and SOHO instruments). The missing pixels are filled by averaging the good values in a 5×5 area around each missing pixel. In the data cubes extracted just 0.04 per cent of the total number of pixels were identified as missing/spikes. The data are then derotated to remove the effects of solar rotation using ROTXY from SOLARSOFT. Finally, from the images that are taken every minute (with a few short gaps), we identify sets of five consecutive images every 15 min and take the average of the five values in each pixel, thus reducing the temporal resolution of the data and the noise of the data. This leaves us with 50 images at 15-min intervals in each data set.

To determine the noise of the data we fit a Gaussian, $G(\psi)$, to the core of a histogram (bin size = 1 Mx cm $^{-2}$) of the distribution of pixel intensities from all frames, $H(\psi)$ (Fig. 2a). Assuming that the core of the distribution is associated with noise then the full-width half-maximum (FWHM) of the fitted Gaussian is equal to the range of the noise. The FWHM is found to be equal to 12.7 Mx cm $^{-2}$. In Fig. 2(b), we plot the survival functions of the observed pixel intensities, $S_{H(\psi)} = 1 - \Sigma H(\psi_i)$ (solid) and the fitted Gaussian core, $S_{G(\psi)} = 1 - \Sigma G(\psi_i)$ (dotted). The ratio of the Gaussian fit over the observed distribution is shown by the dashed line. This plot

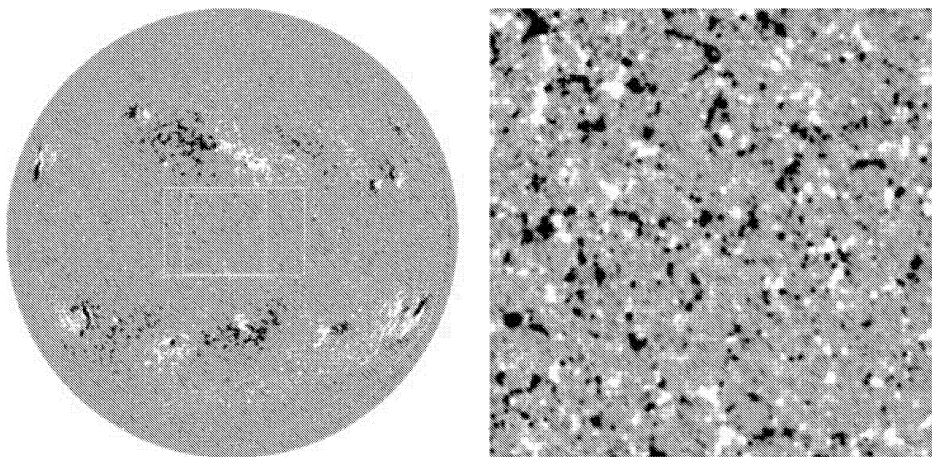


Figure 1. The circular image is a full-disc magnetogram taken by SOHO/MDI on 1998 June 13. The large white rectangle outlines the high-resolution field of view of MDI, whilst the square outlines the area investigated. The right-hand square, 363×363 arcsec 2 in area, is cut from the high-resolution magnetogram taken by MDI at about the same time as the full-disc image. In both images the colours saturate at ± 25 Mx cm $^{-2}$.

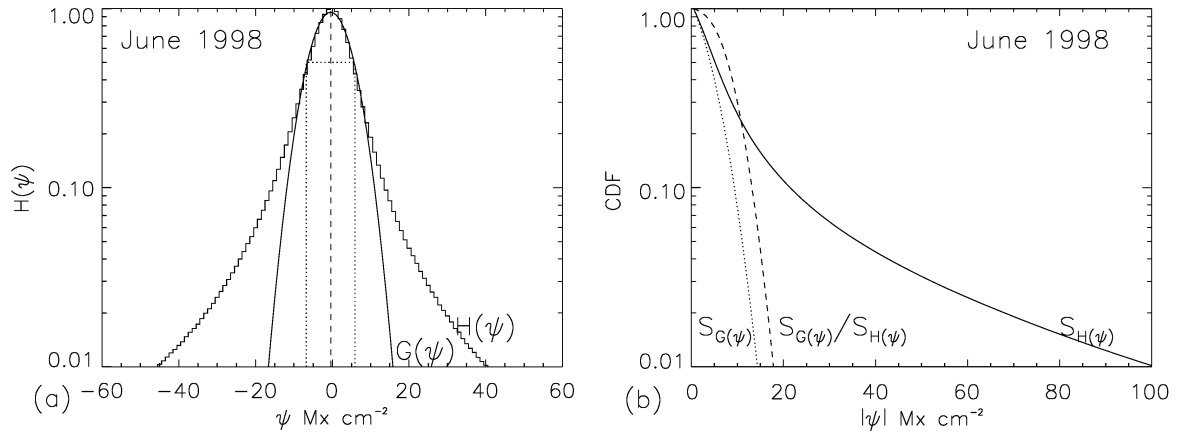


Figure 2. (a) Distribution of the magnetic flux densities (solid). The Gaussian is the fit to the core of the intensity distribution. The dashed lines indicate the centre of the Gaussian, whilst the dotted line shows the FWHM. (b) Survival function for the magnetic flux densities, $S_H(\psi)$, (solid), the fitted Gaussian, $S_G(\psi)$, (dotted) and $S_G(\psi)/S_H(\psi)$ (dashed).

shows that 90 per cent of the noise is less than 10 Mx cm^{-2} and that the fraction of pixels associated with noise falls off steeply. Indeed, above 18 Mx cm^{-2} , less than 1 per cent of the pixels are associated with noise.

To identify the concentrations of flux we choose the following approach. First, all pixels with flux densities greater than a certain level, $\lambda - \sigma$, are identified, where λ is a cut-off and σ is associated with the noise of the data and is equal to half the FWHM of the Gaussian fitted to the core of the flux density distribution. We choose λ to be 25 Mx cm^{-2} and σ to be 6.5 Mx cm^{-2} such that $\lambda - \sigma$ is equal to 18.5 Mx cm^{-2} , and more than 99 per cent of the pixels considered are not associated with noise. Adjacent pixels with flux density greater than $\lambda - \sigma$ are then grouped and uniquely labelled using integers. To be counted as a concentration a group must have at least three pixels and at least one of these pixels must have a flux density greater than λ . Furthermore, we also compare the concentrations in consecutive frames. Each concentration must last for at least three frames before it is counted as a real concentration. Over its lifetime a concentration must have a peak flux density greater than λ at least once during its life, but may in the first few or last few frames of its life just have a peak flux density of greater than $\lambda - \sigma$.

3 MAGNETIC FLUXES

A total of 27 499 concentrations are found in the 50 frames of our data set, making an average of roughly 550 concentrations identified in each frame. For each concentration its area, peak flux density and total flux are calculated. Fig. 3 shows log–log plots of the fluxes versus area and peak flux density of the concentrations. Clearly, the data appear to be highly correlated, except where the fluxes are small. This is especially clear in the flux versus peak flux density plot where the fluxes observed are a lot less than predicted by the correlation of larger fluxes. The reason for this departure is probably because, when the peak flux density is not much larger than λ , the cut-off, the area and flux of the concentration are underestimated. In the case of larger concentrations any pixels with flux just less than $\lambda - \sigma$ that are not counted will only change the area and flux of the concentration by a few per cent, whereas for small concentrations these additional pixels could more than double the area and flux estimated. As a result, we consider only those concentrations that have flux a factor of 3 times larger than would be contained in a ring of pixels of value $(\lambda - \sigma)/2$ that completely surrounds the concentration. This essentially means we only consider those

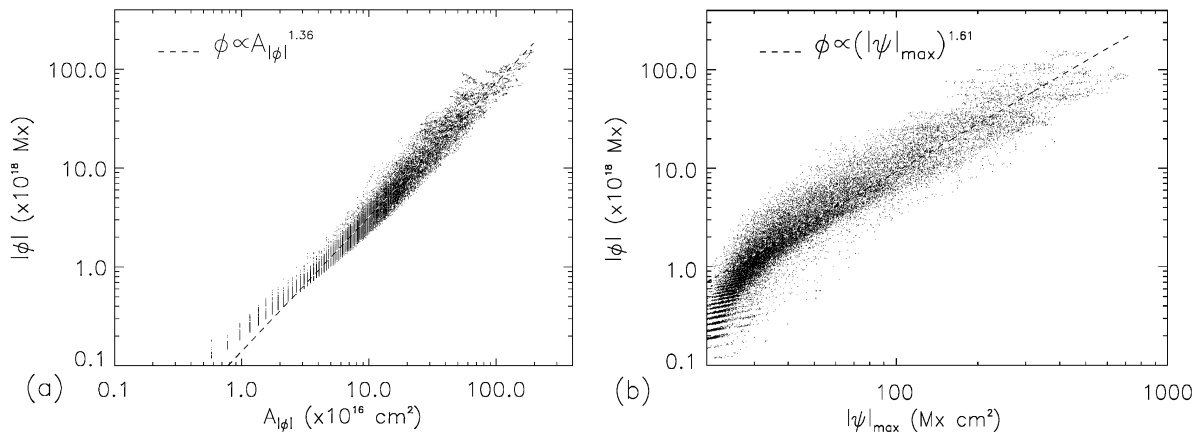


Figure 3. Log–log plots of absolute concentration flux versus concentration (a) area and (b) peak flux density. The dashed lines are fits to the fluxes with $\phi > 6.5 \times 10^{17} \text{ Mx}$.

concentrations with flux greater than 6.5×10^{17} Mx, which leaves us with a total of 22 999 concentrations with approximately 460 in each frame.

3.1 Distribution of fluxes

3.1.1 Probability density functions

The distribution of concentration fluxes is of great potential interest, because it contains information on the rates/balance of fragmentation, coalescence, cancellation and emergence that occur in the magnetic carpet. In the past authors have found, over a small range of fluxes ($10^{18} < |\phi| < 7 \times 10^{18}$ Mx), that the distribution can be considered to be exponential (Schrijver et al. 1997). On the other hand, Wang et al. (1995) found that, if intranetwork and network concentration fluxes are counted separately, then a power law can be fitted to both flux distributions over a limited range (less than an order of magnitude in extent in both cases) which corresponded to less than 50 per cent of the observed concentrations in both cases. Since flux from intranetwork, network, ephemeral region and active-region fields all interact, we need to determine the distribution of all the fluxes over their entire range, to understand the real balance of behaviour in the photosphere.

From a log–linear plot of the histogram of the concentration fluxes (Fig. 4a), it is clear that, if all concentrations are considered, the fluxes do not come from an exponential population. Instead, there are more concentrations with both small and large fluxes than would be anticipated by an exponential probability density function (PDF). Similarly, from a log–log plot of a histogram (Fig. 4b) it is not clear that they come from a power law either, since there appear to be too few small fluxes and too few large fluxes in comparison with a power-law PDF. However, a power law looks the most promising out of these two distributions so we consider this and the best known two-parameter PDF that has this form, known as a Weibull.

A power-law PDF has the form

$$f(\phi; \phi_0, \alpha) = \begin{cases} 0 & 0 \leq |\phi| < \phi_0 \\ (\alpha - 1)(|\phi|/\phi_0)^{-\alpha}/\phi_0 & \phi_0 \leq |\phi| < \infty, \end{cases} \quad (1)$$

where $\alpha > 1$, whilst a Weibull PDF looks like

$$f(\phi; \phi_0, \beta, \gamma) = \begin{cases} 0 & 0 \leq |\phi| < \phi_0 \\ (\gamma/\beta) \left(\frac{|\phi| - \phi_0}{\beta} \right)^{\gamma-1} \\ \times \exp \left[- \left(\frac{|\phi| - \phi_0}{\beta} \right)^\gamma \right] & \phi_0 \leq |\phi| < \infty. \end{cases} \quad (2)$$

Here $\beta, \gamma > 0$. In the determination of the fluxes of the concentrations, we restrict our smallest concentration to be one with three pixels with $|\psi| \geq \lambda - \alpha$ and at least one pixel with $|\psi| \geq \lambda$, so for our data the minimum flux, ϕ_0 , equals 1.07×10^{17} Mx. However, we have shown that the majority of concentrations with fluxes less than 6.5×10^{17} Mx have had their fluxes underestimated and so we set the minimum flux as $\phi_0 = 6.5 \times 10^{17}$ Mx. Hence, the power-law PDF has just one unknown parameter, α , which is known as a shape parameter, and determines the slope of the power law. The Weibull PDF has two unknowns: β , which is a scale parameter and simply ‘scales’ the distributions and γ , which is a shape parameter. In the Weibull PDF, if the shape parameter equals 1 then an exponential distribution is recovered, if it is less than 1 then the distribution has excess small and large fluxes in comparison with an exponential and if it is greater than 1 then a skewed Gaussian distribution is found. Here, we, therefore, expect our estimate of γ to be less than 1.

We now need to estimate the parameters for each of the PDFs to find the ‘best-fitting’ PDF of a particular type. There are many approaches to finding the ‘best-fitting’ PDF of a particular type to a set of data. Graphically one can try and plot a histogram of the data such that a straight line is obtained and then, using least squares or a similar method, a line can be fitted to the data. This method, however, is subjective and also, to create a reasonable number of points after binning requires a large data set. The results can vary depending on the bin size used and, if the data are plotted on log plots, care needs to be taken to make sure an appropriate weighting is chosen for the points, since deviations from the fit that look large at one end of the graph may in fact only be very small owing to the non-linear scaling of a log plot. Finally, for more complicated distributions than exponential and power-law distributions it can be almost impossible to obtain a straight line!

A much better approach, favoured by statisticians, is to use maximum likelihood, which can be performed reliably with both small and large data sets. This involves finding the maximum of the

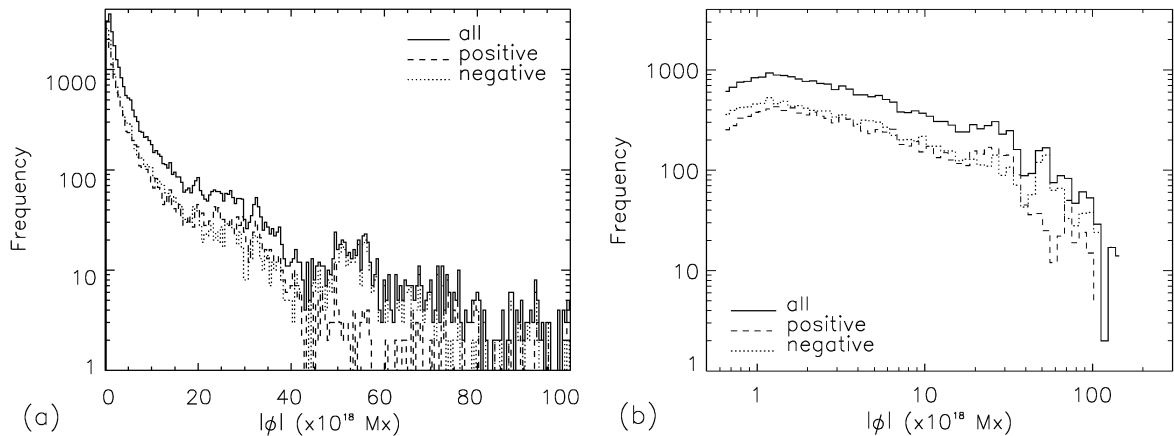


Figure 4. Histogram plotted on a (a) log–linear and (b) log–log graph showing frequency against flux, $|\phi|$ for all concentrations with flux $\phi > 6.5 \times 10^{17}$ Mx.

Table 1. Maximum-likelihood estimates of the parameters for the best-fitting PDFs of a particular form. The errors on the means equal the standard deviation of the estimates from all 50 data sets.

PDF		Maximum-likelihood estimates	
		Positive	Negative
Power law	$\hat{\alpha}$	1.59 ± 0.02	1.59 ± 0.01
Weibull	$\hat{\beta} (\times 10^{18} \text{ Mx})$	5.06 ± 0.43	5.04 ± 0.23
	$\hat{\gamma}$	0.65 ± 0.02	0.60 ± 0.02

log-likelihood of the PDF. The underlying assumption is that the observables, x_i , are independent and, therefore, their probabilities can be multiplied, or equivalently the logs of their probabilities can be added. The maximum-likelihood determines which values of the parameters α_k give us the maximum probabilities for the set of observed ϕ_i . For all the PDFs mentioned above the maximum-likelihood equations are easily derived and can be solved either analytically, in the case of the power law, or numerically, in the other cases. Derivations of the equations for the PDF parameters are given in Appendix A.

As has already been mentioned for the maximum-likelihood method, the data are assumed to be independent. We actually have a series of frames of images in which the fluxes in the first frame are related to those in the next, and so on. We, therefore, derive the estimates of the PDF parameters using just the set of fluxes in one frame and consider each frame in turn to ensure the fluxes are independent. The mean maximum-likelihood estimates for the best-fitting power law and Weibull PDFs are given in Table 1. From the standard deviations of the estimates it is clear that there is no significant difference between each frame.

3.1.2 Goodness of fit

Having found estimates for the parameters of the best-fitting PDFs, we then ask the question, ‘Do the data really come from a population distributed in any of these forms?’. As has already been suggested, this question is not the same as the first question. One of the easiest ways of answering it is to apply a chi-squared test. Chi-squared tests are not very powerful and require the data to be binned, which means that the results are subjective and require a large data set. Since the tests are simple and easy to use, many non-statisticians tend to use

them. However, for common distributions, such as those discussed here, there are many more powerful tests that can be applied that use all the data and are equally easy to use. These tests involve comparing the fitted cumulative distribution function (CDF) with the empirical distribution function (EDF). The CDF, $F(\Phi)$, represents the fraction of fluxes less than or equal to Φ and is calculated from the PDF, $f(\phi)$

$$F(\Phi) = \int_0^{\Phi} f(x) dx. \quad (3)$$

Analogously, the EDF for a particular data set represents the fraction of observed fluxes less than or equal to Φ . If we sort all the data into increasing order such that $0 < \phi_1 < \dots < \phi_i < \dots < \phi_n < \infty$, then, if $\Phi = \phi_i$, there are i/n fluxes with flux less than or equal to Φ . For technical reasons, i is replaced by $i - \frac{1}{2}$ and the EDF is defined as

$$F_i = (i - 1/2)/n; \quad i = 1, \dots, n. \quad (4)$$

A graphical approach to comparing these distributions is to consider a plot of the CDF, $F(\phi_i)$, against the EDF, F_i . Such a plot is called a P–P plot. If the two distributions were the same then we would expect to obtain a straight line through the origin. From Fig. 5(a), we see that the best-fitting power law (dotted) is clearly not as good a fit as the best-fitting Weibull (dashed). For interest, Fig. 5(b) shows a graph of the two survival functions $[1 - F(\phi)]$ plotted against flux. The EDF is also included on this graph for comparison.

The quantitative value we use to determine the goodness of fit of the fitted PDFs to our fluxes is the Kolmogorov–Smirnov, D , statistic which is equal to

$$D = \max|F(\phi_i) - F_i|. \quad (5)$$

For a sample size, n , where $n > 100$, if $D < D_{0.05} = \sqrt{\ln(2/0.05)/2n} = 1.358/\sqrt{n}$, then we conclude that, at the 5 per cent significance level, the data are consistent with the specified distribution proposed. This means we cannot say for sure that the data come from a particular distribution, just that we cannot reject that hypothesis. Typically, there are about 200 fluxes of one polarity in each frame, hence, the typical value of $D_{0.05}$ is approximately 0.096. For the power-law fits, the mean D statistics are 0.13 and 0.11, respectively, for the positive and negative fluxes and so it is not a surprise to find that in all the cases, we can reject

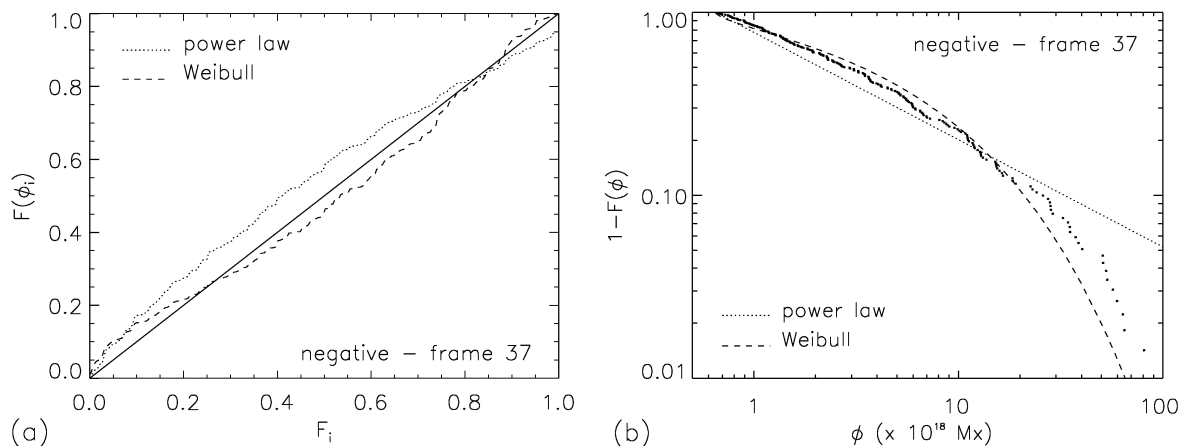


Figure 5. Comparison of the best-fitting CDFs to the observed EDF for the negative fluxes in frame 37: (a) a P–P plot of the CDFs, $F(\phi_i)$, versus the EDF, F_i , and (b) the survival functions, $1 - F(\phi)$, versus flux, ϕ .

Table 2. Estimates of the mean total flux density predicted by the best-fitting PDFs of a particular form.

PDF	Total flux density	
	Positive	Negative
Power law	$T_p = \infty \text{ Mx cm}^{-2}$	$T_n = \infty \text{ Mx cm}^{-2}$
Weibull	$T_p = 2.30 \text{ Mx cm}^{-2}$	$T_n = 2.93 \text{ Mx cm}^{-2}$
Observed	$T_p = 2.42 \text{ Mx cm}^{-2}$	$T_n = 3.18 \text{ Mx cm}^{-2}$

the hypothesis that data come from a power-law population. The D statistics for the Weibull PDFs have means of 0.075 and 0.079, respectively, for the positive and negative fluxes with 88 and 78 per cent of the 50 frames having D statistics below the $D_{0.05}$ for that frame. This means that, in the majority of cases, we cannot reject the hypothesis that the fluxes come from a population distributed in the form of a Weibull.

3.1.3 Total flux density

The mean total flux density can be easily determined for both the positive and negative concentrations. The observed total flux density for the positive and negative concentrations with flux greater than $6.5 \times 10^{17} \text{ Mx}$ is 2.42 Mx cm^{-2} and -3.18 Mx cm^{-2} , respectively. For the PDFs, we can determine the total flux density in the region by solving the equation

$$T = \int_0^{\infty} \phi f(\phi) d\phi.$$

Table 2 shows that the Weibull PDF produces good predictions that are greater than 92 per cent of the observed values. The power-law PDF does not give reasonable estimates, because its index is less than 2 and so the large flux concentrations at infinity dominate.

4 DISCUSSION

4.1 Consideration of biases

All the analysis so far has been on concentrations that have a minimum area of $5.9 \times 10^{15} \text{ cm}^2$ (three MDI high-resolution pixels), have a minimum flux of $6.5 \times 10^{17} \text{ Mx}$ and last for at least three frames (45 min). Clearly, this last constraint can be improved upon significantly since the data have a cadence of 1 min and, therefore, to investigate its effect on our results we run through all our analysis again on a set of 50 frames that are just 5 min apart. This time we find 31 379 concentrations with 25 862 of them having absolute flux

greater than $6.5 \times 10^{17} \text{ Mx}$. Table 3 shows the mean maximum-likelihood estimates for the PDFs tested, as well as the mean Kolmogorov–Smirnov D statistic and the percentage of fits that have a D statistic less than $D_{0.05}$. In the table, the mean predicted values of the total flux density are given, as well as their fraction with respect to the observed values of 5.70 Mx cm^{-2} for the total absolute flux density and 2.39 and 3.31 Mx cm^{-2} for the positive and negative total flux densities, respectively.

As one might expect, by reducing the minimum lifetime of the concentrations more small-flux concentrations are observed and these lead to a slight increase in the power-law index, $\hat{\alpha}$. However, we find that a power law is still not a good fit to the distribution of fluxes. From Table 3, we see that overall the Weibull PDF once again gives both a good fit to the data and a reasonable estimate of the total flux density. By increasing the numbers of small fluxes we find that in the Weibull PDF the value of $\hat{\beta}$, the scale parameter, decreases, whilst the shape parameters $\hat{\gamma}$ varies only slightly.

4.2 Physical interpretation

The above results suggest that a Weibull PDF is a reasonable estimate of the distribution of fluxes (Fig. 6a), but what does such a distribution imply concerning the processes that occur in the magnetic carpet? As has already been said, the emergence of new flux is observed to be distributed in the form of an exponential, $\exp[-1.6 \times 10^{-19}(|\phi_+| + |\phi_-|)]$ (Hagenaar 2001). Assuming, for simplicity, that the distribution of new positive concentrations is the same as that for negative concentrations then $E(\phi) \propto \exp(-1.6 \times 10^{-19}|\phi|)$. Emergence of flux occurs over a wide range of scales from 10^{17} to 10^{19} Mx or more. Physically, the observed distribution of fluxes can be thought of as having three elements (Fig. 6b).

- (1) Emergence over all scales produces an initial exponential distribution over a wide range of fluxes.
- (2) Fragmentation and partial cancellation breakup concentrations and produce smaller and smaller fluxes thus producing additional small fluxes. Support for this idea comes from the two-dimensional magnetic carpet models of Parnell (2001), which were used to show that a high fragmentation rate leads to a steepening of the distribution at low fluxes.
- (3) Coalescence and the injection of fluxes from remnants of active regions tends to produce larger fluxes and therefore additional large fluxes are created.

This idea is an alternative to that put forward by (Schrijver et al. 1997) who suggested that flux was injected at either end of the flux

Table 3. Maximum-likelihood estimates, Kolmogorov–Smirnov D statistics and predicted total flux densities for the best-fitting PDFs of a particular form for the data determined assuming a cadence for the frames of 5 min. The errors on the means equal the standard deviation of the estimates from all 50 data sets. ϕ_0 is assumed to be $6.5 \times 10^{17} \text{ Mx}$.

PDF	Maximum-likelihood estimates, Kolmogorov–Smirnov statistics and total flux densities		
		Positive	Negative
Power law	$\hat{\alpha}$	1.63 ± 0.02	1.62 ± 0.01
	D (per cent of D 's with $D < D_{0.05}$)	0.12 ± 0.02 (0 per cent)	0.10 ± 0.01 (2 per cent)
	T [Mx cm^{-2}]	∞	∞
Weibull	$\hat{\beta}$ [$\times 10^{18} \text{ Mx}$]	4.27 ± 0.25	4.50 ± 0.20
	$\hat{\gamma}$	0.64 ± 0.02	0.59 ± 0.01
	D (per cent of D 's with $D < D_{0.05}$)	0.07 ± 0.01 (90 per cent)	0.08 ± 0.01 (58 per cent)
	T [Mx cm^{-2}] (T/T_{obs})	2.26 (0.95)	3.03 (0.92)

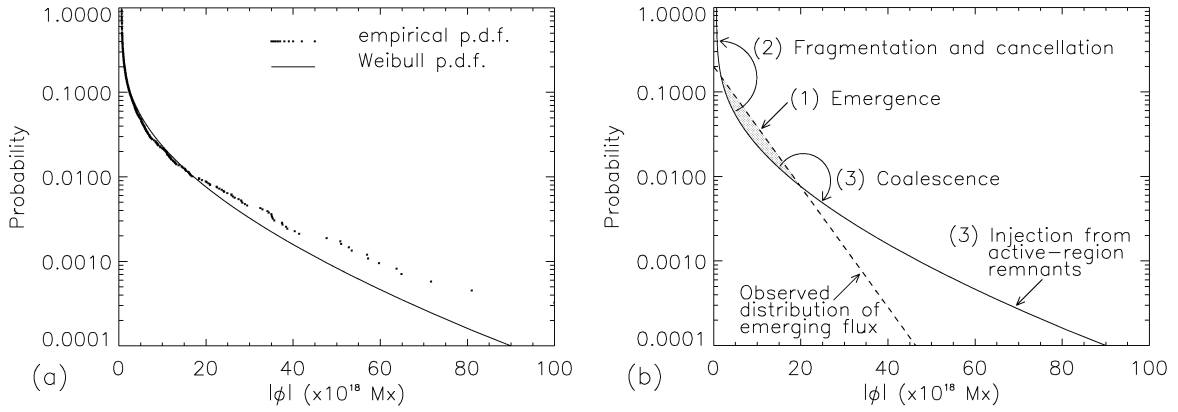


Figure 6. (a) Log–linear plot of the fitted Weibull PDF (solid) and the empirical CDF versus flux. (b) Sketch showing the physical interpretation of the Weibull PDF (solid). The dashed line has the same slope as the observed emerging flux distribution, $E(\phi) \approx \exp(-1.6 \times 10^{-19}|\phi|)$. This flux is redistributed by the processes labelled to give a Weibull.

range and that coalescence created large fluxes from the injected small fluxes and fragmentation broke up the injected large fluxes into small fluxes creating an exponential distribution over the entire range of fluxes.

Schrijver et al. (1997), defined equations of ‘magneto-chemistry’ for the balance between emergence, cancellation, coalescence and fragmentation. These equations model the effects of the spatially averaged rates of the four processes on the number of fluxes. They found a few simple solutions, but we find that, if the number of fluxes is in equilibrium, the rates of each process are not necessarily the same for both polarities and there is a detailed balance between the processes, then there is a whole range of possible solutions to the equations, including ones for fluxes distributed in the form of a Weibull distribution.

First, like Schrijver et al. (1997), we assume that the flux that cancels simply returns as a newly emerged flux such that the emergence rate, $E(\phi)$, equals the cancellation rate, $C(\phi)$,

$$C(\phi) = N_+(\phi) \int_0^\infty N_-(\phi+x) m_-(\phi+x, \phi) dx + N_-(\phi) \int_0^\infty N_+(\phi+x) m_+(\phi+x, \phi) dx, \quad (6)$$

where, $N_\pm(\phi) = n_\pm f_\pm(\phi)/A$ ($\text{Mx}^{-1} \text{cm}^{-2}$), n_\pm is the total number of positive (negative) concentrations in area A and $f_\pm(\phi)$ is the PDF of the positive (negative) fluxes. The rate of cancellation of fluxes $\phi_{1\pm}$ and $\phi_{2\mp}$, where $|\phi_{1\pm}| > |\phi_{2\mp}|$ is denoted by $m_\pm(\phi_1, \phi_2)$. This rate is dependent on the sign of the fluxes, since it is likely to depend on the densities of the fluxes. If we assume that all the cancelled flux reappears then the cancellation and emergence terms can be written as a pair of terms that effectively act like fragmentation. Assuming a steady state, the balance between emergence, cancellation, fragmentation and coalescence can be written as

$$\begin{aligned} & \frac{1}{2} \int_0^\phi N_\pm(x) N_\pm(\phi-x) l_\pm(x, \phi-x) dx \\ & - N_\pm(\phi) \int_0^\infty N_\pm(x) l_\pm(\phi, x) dx \\ & + 2 \int_0^\infty N_\pm(\phi+x) [k_\pm(\phi, x) + q_\pm(\phi, x)] dx \\ & - N_\pm(\phi) \int_0^\phi k_\pm(x, \phi-x) + q_\pm(x, \phi-x) dx = 0, \quad (7) \end{aligned}$$

where

$$q_\pm(\phi_1, \phi_2) \equiv [N_\mp(\phi_1) m_\pm(\phi_1 + \phi_2, \phi_1) + N_\mp(\phi_2) m_\pm(\phi_1 + \phi_2, \phi_2)]/2,$$

and $l_\pm(\phi_1, \phi_2)$ is the coalescence rate, $k_\pm(\phi_1, \phi_2)$ is the fragmentation rate and $m_\pm(\phi_1, \phi_2)$ is the cancellation rate. Equation (7) here is the same as equation (5) in Schrijver et al. (1997) except for the additional possibility that the rates of each process may be dependent on the polarity of the concentrations involved. The first and second terms in equation (7) represent the gain and loss, respectively, owing to cancellation and the third and fourth terms are the gain and loss, respectively, owing to fragmentation and cancellation/emergence.

Schrijver et al. (1997) noted that in the case of detailed balance between all the processes the above equation has the well-known exact solution

$$N_\pm(\phi_1) N_\pm(\phi_2) l_\pm(\phi_1, \phi_2) = 2N_\pm(\phi_1 + \phi_2) [k_\pm(\phi_1, \phi_2) + q_\pm(\phi_1, \phi_2)]. \quad (8)$$

In their paper, Schrijver et al. (1997) discussed some very simple forms of equation (8) where the fragmentation rate, $k(\phi_1, \phi_2) = k_0$, and the coalescence and cancellation rates, $l(\phi_1, \phi_2) = m(\phi_1, \phi_2) = l_0$, are constant. However, there are many other forms that this equation can take. Here, we consider just one set to show that a Weibull distribution can easily be obtained.

For number densities of fluxes of the form $N_\pm(\phi) = n_\pm f_\pm(\phi)/A$, we find that the exact solution above is satisfied if the rates of fragmentation, coalescence and cancellation are of the form

$$\begin{aligned} k_\pm(\phi_1, \phi_2) &= \frac{k_0}{2A} f_\pm(\phi_1) f_\pm(\phi_2) g_\pm(\phi_1, \phi_2), \\ l_\pm(\phi_1, \phi_2) &= \frac{3k_0}{n_\pm} f_\pm(\phi_1 + \phi_2) g_\pm(\phi_1, \phi_2), \\ m_\pm(\phi_1, \phi_2) &= \frac{k_0}{n_\mp} \frac{f_\pm(\phi_1 - \phi_2) f_\pm(\phi_2)}{f_\mp(\phi_2)} g_\pm(\phi_1 - \phi_2, \phi_2), \end{aligned}$$

where $g_\pm(\phi_1, \phi_2)$ can be any function of ϕ_1 and ϕ_2 that satisfies $g_\pm(\phi_1, \phi_2) = g_\pm(\phi_2, \phi_1)$. Note, that these solutions imply that the rates of each process are different for the positive and negative concentrations, as one would imagine if the PDFs of the two species are different. Owing to the detailed balance, the rate of fragmentation is dependent on the PDF of the two fluxes that result from the fragmentation, the rate of coalescence is dependent on the PDF of the flux that is created through coalescence and the rate of

cancellation depends on the PDF of the flux remaining after cancellation. These dependences are all physically reasonable under the assumption of detailed balance. Clearly, without constraints for $k_{\pm}(\phi_1, \phi_2)$, $l_{\pm}(\phi_1, \phi_2)$ and $m_{\pm}(\phi_1, \phi_2)$ a PDF of any form is a solution to equation (7) and, therefore, the assumptions of equilibrium and detailed balance are not major constraints on the distribution of fluxes. Indeed, at least three of the following: number density of fluxes, or any of the rates of the four magnetic carpet processes are needed to prove or disprove the assumptions.

For example, assuming that the PDFs for the positive and negative fluxes are known and that the distribution of positive and negative emerged/cancelled concentrations is exponential (Hagenaar 2001), we can then choose the function $g(\phi_1, \phi_2)$ to be, for example,

$$g_{\pm}(\phi_1, \phi_2) = \frac{\exp(-(\phi_1 + \phi_2)/\eta_{\pm})}{f_{\pm}(\phi_1)f_{\pm}(\phi_2)f_{\pm}(\phi_1 + \phi_2)}.$$

This leads to a rate of emergence and cancellation of the form,

$$E(\phi) = C(\phi) = \frac{n_+ k_0 \eta_+}{A^2} \exp(-\phi/\eta_+) + \frac{n_- k_0 \eta_-}{A^2} \exp(-\phi/\eta_-), \quad (9)$$

where the exponential slopes of the positive and negative fluxes are $-1/\eta_+$ and $-1/\eta_-$, respectively. Clearly, the emergence rate is distributed in the form of an exponential and the rates of fragmentation, coalescence and cancellation, respectively, have the following forms:

$$k_{\pm}(\phi_1, \phi_2) = \frac{k_0}{2A} \frac{\exp(-(\phi_1 + \phi_2)/\eta_{\pm})}{f_{\pm}(\phi_1 + \phi_2)},$$

$$l_{\pm}(\phi_1, \phi_2) = \frac{3k_0}{n_{\pm}} \frac{\exp(-\phi_1/\eta_{\pm}) \exp(-\phi_2/\eta_{\pm})}{f_{\pm}(\phi_1)f_{\pm}(\phi_2)},$$

$$m_{\pm}(\phi_1, \phi_2) = \frac{k_0}{n_{\mp}} \frac{\exp(-\phi_1/\eta_{\pm})}{f_{\pm}(\phi_1)f_{\mp}(\phi_2)}.$$

If the PDF, $f(\phi)$ is in the form of a Weibull PDF (equation 2), then these rates become

$$\begin{aligned} k_{\pm}(\phi_1, \phi_2) &= \frac{k_0 \beta_{\pm}}{2A \gamma_{\pm}} \left(\frac{\phi_1 + \phi_2 - \phi_0}{\beta_{\pm}} \right)^{1-\gamma_{\pm}} \\ &\quad \times \exp \left[\left(\frac{\phi_1 + \phi_2 - \phi_0}{\beta_{\pm}} \right)^{\gamma_{\pm}} - \frac{\phi_1 + \phi_2}{\eta_{\pm}} \right], \\ l_{\pm}(\phi_1, \phi_2) &= \frac{3k_0 \beta_{\pm}^2}{n_{\pm} \gamma_{\pm}^2} \left(\frac{\phi_1 - \phi_0}{\beta_{\pm}} \right)^{1-\gamma_{\pm}} \left(\frac{\phi_2 - \phi_0}{\beta_{\pm}} \right)^{1-\gamma_{\pm}} \\ &\quad \times \exp \left[\left(\frac{\phi_1 - \phi_0}{\beta_{\pm}} \right)^{\gamma_{\pm}} + \left(\frac{\phi_2 - \phi_0}{\beta_{\pm}} \right)^{\gamma_{\pm}} - \frac{\phi_1 + \phi_2}{\eta_{\pm}} \right], \\ m_{\pm}(\phi_1, \phi_2) &= \frac{k_0 \beta_{\pm} \beta_{\mp}}{n_{\mp} \gamma_{\pm} \gamma_{\mp}} \left(\frac{\phi_1 - \phi_0}{\beta_{\pm}} \right)^{1-\gamma_{\pm}} \left(\frac{\phi_2 - \phi_0}{\beta_{\mp}} \right)^{1-\gamma_{\mp}} \\ &\quad \times \exp \left[\left(\frac{\phi_1 - \phi_0}{\beta_{\pm}} \right)^{\gamma_{\pm}} + \left(\frac{\phi_2 - \phi_0}{\beta_{\mp}} \right)^{\gamma_{\mp}} - \frac{\phi_1}{\eta_{\pm}} \right]. \end{aligned}$$

This means that the hypothesis that (i) the fluxes are distributed in the form of a Weibull PDF, (ii) the emerging flux is distributed in the form of an exponential, and (iii) the fluxes are in detailed balance can, in future, be tested if the spatially averaged rate of

fragmentation or cancellation or coalescence for the positive and negative concentrations are determined.

5 CONCLUSIONS

An automated detection algorithm has been used to investigate the distribution of fluxes from magnetic concentrations in the magnetic carpet. A region of area 363×363 arcsec² (264×264 Mm²) has been studied for 12 h with frames every 15 min. In total, we observed 27 500 concentrations, making an average of roughly 550 concentrations identified in each frame. The concentrations had a median flux of approximately 2×10^{18} Mx, a median area of approximately 7×10^{16} cm² and a median peak flux density of about 36.0 Mx cm⁻². The mean values of these properties are, in all cases, larger than their median values by about a factor of 3. These averages imply that the distributions of these characteristics have a high degree of positive skewness and, therefore, have extended tails at high fluxes.

The distribution of the concentration fluxes is of particular interest. Papers have previously suggested that the distribution of fluxes is either exponential or in the form of a power law, but, in both cases only a limited range of fluxes was considered, extending over less than an order of magnitude. Neither of these distributions are very realistic, although, in principle, both can predict a finite absolute flux density, provided suitable parameter values exist. Fluxes extending over three orders of magnitude have been considered here and they clearly show that the distribution of fluxes is neither exponential nor a power law. In particular, it was found that there are excess fluxes at both ends of the distribution in comparison with an exponential, and a lack of fluxes at both tails in comparison with a power law. A well-known two-parameter PDF that behaves in this fashion is the Weibull PDF. It has a combination of an exponential and power-law term and gives a significantly better fit than either the exponential or power-law PDFs alone. In terms of the Kolmogorov–Smirnov goodness-of-fit statistic, D , the hypothesis that the fluxes come from a population distributed with a Weibull PDF cannot be rejected with a 5 per cent significance level. Furthermore, on physical grounds, the Weibull distribution does much better than the power law by predicting the total flux density with estimates within 8 per cent of those observed. We, therefore, conclude that the Weibull PDF, out of these well-known single one- and two-parameter distributions, is the best fit to the observed distribution of fluxes. However, it is worth noting that the fluxes may actually come from two separate distributions and that this may give an even better fit.

We explain the observed excess of fluxes at both ends in comparison with an exponential as being the result of fragmentation/cancellation and coalescence on an initially exponential distribution of emerged concentrations. If we suppose that the distribution of emerged concentrations is in the form of an exponential, as suggested by Hagenaar (2001), then fragmentation and partial cancellation will tend to form smaller and smaller concentrations leading to extra small fluxes. The two-dimensional models of the magnetic carpet produced by Parnell (2001) showed that if the fragmentation rate is large this is indeed what happens. Coalescence and the injection of extra flux from remnant active regions gives rise to an increase in the numbers of large fluxes, as observed.

The equation of magneto-chemistry proposed by Schrijver et al. (1997) that determines the distribution of fluxes in terms of spatially averaged rates of emergence, cancellation, fragmentation and coalescence is also considered. We show that, by assuming that the distribution of positive and negative fluxes are both in equilibrium, but

not necessarily equal, and that if there is detailed balance between the processes, then there are many physically realizable solutions to this equation. One particular example is discussed that produces the observed flux distribution and the observed exponential distribution of emerged fluxes, but these two observables alone are not enough to determine all the process rates. In addition, the observed rate of at least one of the other processes is needed. We have therefore produced a set of equations that can, in future, be used to test whether the magnetic carpet is indeed close to a detailed-balanced equilibrium.

ACKNOWLEDGMENTS

CEP would like to thank the Royal Astronomical Society for her funding by way of the Sir Norman Lockyer Fellowship. Also, the author appreciates the helpful suggestions and useful discussions from Dr Peter Jupp, Professor Eric Priest and Dr Thomas Neukirch.

REFERENCES

- Cattaneo F., 1999, ApJ, 515, L39
 Hagenaar H. J., 2001, ApJ, 555, 448
 Hagenaar H. J., Schrijver C. J., Title A. M., Shine R. A., 1999, ApJ, 511, 932
 Harvey K. L., 1984, Proc. 4th European Meeting on Solar Physics. The Hydromagnetics of the Sun, ESA SP, 220, 235
 Harvey K. L., Harvey J. W., 1976, in Martin S. F., Harvey K. L., eds, Part II Air Force Report AFGL-TR-76-0225, 35
 Harvey K. L., Martin S. F., 1973, Solar Phys., 32, 389
 Harvey J. W., Harvey K. L., Martin S. F., 1975, Solar Phys., 40, 87
 Harvey K. L., Jones H. P., Schrijver C. J., Penn M. J., 2000, Solar Phys., 190, 35
 Livi S. H. B., Martin S. F., Wang J., 1985, Australian J. Phys., 38, 855
 Livingston W. C., Harvey J. W., 1975, Bull. Amer. Astron. Soc., 7, 346
 Martin S. F., 1984, in Keil S. L., ed., Proc. Symp. on Small-Scale Dynamical Processes in Quiet Stellar Atmospheres, 30
 Martin S. F., 1988, Solar Phys., 117, 243
 Martin S. F., 1990, in Stenflo J.O., ed., Solar Photosphere, Structure, Convection and Magnetic Fields, 129
 Parnell C. E., 2001, Solar Phys., 200, 23
 Scherrer P. H. et al., 1995, Solar Phys., 162, 129
 Schrijver C. J., Harvey K. L., 1994, Solar Phys., 150, 1
 Schrijver C. J., Title A. M., van Ballegooyen A. A., Hagenaar H. J., Shine R. A., 1997, ApJ, 487, 424
 Title A., 2000, Phil. Trans. R. Soc. Lond. A, 358, 657
 Wang H., 1988, Solar Phys., 117, 343
 Wang J., Shi Z., 1988, Acta. Astron. Sinica., 29, 48
 Wang H., Zirin H., 1988, Solar Phys., 115, 205
 Wang H., Zirin H., Shi Z., 1985, Solar Phys., 98, 241
 Wang J., Wang H., Tang F., Lee J. W., Zirin H., 1995, Solar Phys., 160, 277
 Webb D. F., Martin S. F., Moses D., Harvey J. W., 1993, Solar Phys., 144, 15
 Zirin H., 1985, Australian J. Phys., 38, 961
 Zirin H., 1987, Solar Phys., 110, 101
 Zwaan C., 1987, Ann. Rev. A&A, 25, 83

APPENDIX A: MAXIMUM-LIKELIHOOD ESTIMATES

The log-likelihood of an m -parameter PDF, $f(x; \alpha_1, \dots, \alpha_m)$, for a sample of n observables, x_i , is equal to

$$l(\alpha_1, \dots, \alpha_m; x_1, \dots, x_n) = \sum_{i=1}^n \ln f(x_i, \alpha_1, \dots, \alpha_m).$$

The maximum-likelihood method maximizes the probabilities of all the observed x_i and so the following equations determine the estimates of the parameters:

$$\frac{dl(\alpha_1, \dots, \alpha_m; x_1, \dots, x_n)}{d\alpha_k} = 0 \quad k = 1, \dots, m.$$

These equations can be solved either analytically or numerically to provide the maximum-likelihood estimates, $\hat{\alpha}_1, \dots, \hat{\alpha}_m$, of the parameters $\alpha_1, \dots, \alpha_m$ of the best-fitting PDF.

A1 Maximum-likelihood estimation of the power-law index

As has already been stated in Section 3.1 a power-law PDF has one parameter, α , and is of the form

$$f(\phi) = \begin{cases} 0 & 0 \leq |\phi| < \phi_0 \\ (\alpha - 1)(|\phi|/\phi_0)^{-\alpha}/\phi_0 & \phi_0 \leq |\phi| < \infty, \end{cases}$$

where ϕ_0 is assumed to be known. For a sample of n fluxes, $\phi_0 < |\phi_1| < \dots < |\phi_i| < \dots < |\phi_n| < \infty$, the log-likelihood of $f(\phi)$ is equal to

$$\begin{aligned} l(\alpha; \phi_0, \phi_1, \dots, \phi_n) &= \sum_{i=1}^n \ln f(\phi_i) \\ &= \sum_{i=1}^n \left(\ln \frac{\alpha - 1}{\phi_0} - \alpha \ln \frac{|\phi_i|}{\phi_0} \right). \end{aligned}$$

Since, the minimum flux, ϕ_0 , is assumed to be known the only unknown parameter is α , hence, we only have one equation to solve. The maximum value of $l(\alpha, \phi_0, \phi_1, \dots, \phi_n)$ is obtained when $dl/d\alpha = 0$:

$$\begin{aligned} \frac{dl(\alpha; \phi_0, \phi_1, \dots, \phi_n)}{d\alpha} &= \sum_{i=1}^n \left(\frac{1}{\alpha - 1} - \ln \frac{|\phi_i|}{\phi_0} \right) \\ &= \frac{n}{\alpha - 1} - \sum_{i=1}^n \ln \frac{|\phi_i|}{\phi_0} = 0. \end{aligned}$$

The value of α that maximizes the above derivative is the maximum-likelihood estimate $\hat{\alpha}$ and equals

$$\hat{\alpha} = \frac{1}{\text{mean}[\ln(|\phi|/\phi_0)]} + 1. \quad (\text{A1})$$

A2 Maximum-likelihood estimation of the Weibull parameters

The Weibull distribution has a PDF of the form

$$f(\phi) = \begin{cases} 0 & 0 \leq |\phi| < \phi_0 \\ (\gamma/\beta) \left(\frac{|\phi| - \phi_0}{\beta} \right)^{\gamma-1} \\ \quad \times \exp \left[- \left(\frac{|\phi| - \phi_0}{\beta} \right)^\gamma \right] & \phi_0 \leq |\phi| < \infty, \end{cases}$$

where ϕ_0 is assumed known. We, therefore, make the substitution $\phi' = |\phi| - \phi_0$ to reduce the PDF to

$$f(\phi') = (\gamma/\beta) (\phi'/\beta)^{\gamma-1} \exp[-(\phi'/\beta)^\gamma].$$

For our sample of n fluxes, $0 < \phi'_1 < \dots < \phi'_i < \dots < \phi'_n < \infty$, the log-likelihood of $f(\phi')$ is defined as

$$l(\beta, \gamma; \phi'_1, \dots, \phi'_n) = \sum_{i=1}^n \left[\ln \frac{\gamma}{\beta} + (\gamma - 1) \ln \frac{\phi'}{\beta} - \left(\frac{\phi'}{\beta} \right)^\gamma \right].$$

The derivatives of $l(\beta, \gamma, \phi'_1, \dots, \phi'_n)$ are

$$\frac{dl(\beta, \gamma; \phi'_1, \dots, \phi'_n)}{d\beta} = -\frac{n\gamma}{\beta} + \frac{\gamma}{\beta^{\gamma+1}} \sum_{i=1}^n (\phi'_i)^\gamma,$$

$$\begin{aligned} \frac{dl(\beta, \gamma; \phi'_1, \dots, \phi'_n)}{d\gamma} &= \frac{n}{\gamma} + \sum_{i=1}^n \ln \phi'_i - n \ln \beta \\ &\quad - \sum_{i=1}^n \left(\frac{\phi'_i}{\beta} \right)^\gamma \ln \left(\frac{\phi'_i}{\beta} \right). \end{aligned}$$

Setting these equations equal to zero, rearranging and eliminating β from the second equation yields the following equations

$$\hat{\beta} = \left(\frac{\sum_{i=1}^n (\phi'_i)^\gamma}{n} \right)^{1/\hat{\gamma}}, \quad (\text{A2})$$

$$\frac{1}{\hat{\gamma}} + \frac{1}{n} \sum_{i=1}^n \ln \phi'_i - \frac{\sum_{i=1}^n (\phi'_i)^\gamma \ln \phi'_i}{\sum_{i=1}^n (\phi'_i)^\gamma} = 0. \quad (\text{A3})$$

The maximum-likelihood estimates are then gained by solving equation (A3) numerically to give $\hat{\gamma}$ and then using this to find $\hat{\beta}$ from equation (A2).

This paper has been typeset from a $\text{\TeX}/\text{\LaTeX}$ file prepared by the author.